J. Fluid Mech. (1982), *vol.* 115, *pp.* 327–346
Printed in Great Britain

The evolution of disturbances in an Ekman boundary layer

By G. F. SPOONER AND W. O. CRIMINALE†
Department of Oceanography, University of Washington, Seattle, Washington 98195, U.S.A.

(Received 30 July 1980 and in revised form 21 May 1981)

A linear model of a wave packet in a laminar Ekman boundary layer is proposed for tracing the development of an initially localized pulsed perturbation at the boundary. The model disturbance was built up from a linear combination of growing modes summed numerically over all wavenumbers and frequencies. The input spectrum was assumed to be flat so that there was no biasing at any wavenumber or frequency and the evolution was calculated on the basis of linear-stability theory. The wave packet generated by the summation of modes developed uniformly downstream of the disturbance source location and, depending upon the choice of the Reynolds number, vividly displayed results representative of the different kinds of instabilities that are present in the Ekman layer. Outputs in the form of perspective plots are given in order to explain the evolution of the packet into either a single wave patch or a sum of individual wave patches.

1. Introduction

Interest in initial-value problems arises naturally out of the considerations of classical stability theory. Such theory is concerned with the stability of small perturbations, the simplest of which is a small-amplitude wave imposed upon a mean flow. Once the behaviour of the waves has been determined, it is logical to ask what might occur if the original disturbance is of a more general form. The question of how such a disturbance develops and what form it may ultimately assume becomes the central issue of the problem.

To a large extent, the theoretical work that has been done on the growth rates of simple, two-dimensional waves for boundary layers was validated by the experimental work of Schubauer & Skramstad (1948). In these experiments the growth rates and propagation velocities of disturbances in a flat-plate boundary layer were measured and reasonable agreement with the theoretical calculations that were made by Schlichting (1935), based on a quasi-parallel flow treatment, were obtained. The disturbances that occur naturally in such boundary layers are more likely to be of a three-dimensional nature, however. Indeed, this has been demonstrated by Klebanoff, Tidstrom & Sargent (1962). Further, the transition process from laminar to turbulent flow, a phenomenon that has motivated much of the study of the initial-value problem, is highly three-dimensional. In view of these facts, the study of what occurs after the inception of a three-dimensional disturbance, such as a pulse, becomes very attractive.

Investigation of a three-dimensional disturbance in non-rotating flows has been well treated. For example, Criminale (1960) considered the general three-dimensional problem. Benjamin (1961) explored the flow down an inclined plate. Criminale & Kovasznay (1962) treated the problem of a disturbance in a flat-plate Blasius boundary layer. The case of a two-dimensional unbounded parallel flow was considered by Gaster & Davey (1968).

† Also at Applied Mathematics Group, Geophysics Program, University of Washington, Seattle.

More recent work includes the important experimental work of Gaster & Grant (1975). In this experiment, a pulse-like disturbance was introduced into a flat-plate boundary layer, and the resulting velocities measured at a number of downstream stations. The results, for the initial period at least, agreed very well with a theoretical model of the phenomenon given by Gaster (1975).

There should be little doubt as to the importance of the method. Generally speaking, however, the work has not come easily. The calculations cannot be made using standard eigenfunction expansions, as is common with initial-value, boundary-value problems. Even more to the point, not all the possible modes have been determined for any flow stability. The boundary layer, where most of the experimental information is known, has only very recently had the complete eigenvalue spectrum investigated. In particular there is the numerical work of Mack (1976), with Gustavsson (1979) considering the effects by Laplace-transform methods.

The present case differs from these previous investigations in that the mean flow under consideration is that of a rotating boundary layer. Although rotation causes the mean flow to be three-dimensional, along with attendant difficulties, there are several features that make this problem attractive.

First, there is the fact that the velocity profile of the rotating boundary layer, the Ekman spiral, is an exact solution to the Navier–Stokes equation. Second, the Ekman-layer flow is strictly parallel. There is no downstream growth of the boundary layer, obviating any need either to make a local parallel-flow assumption in order to obtain eigenvalues, or to take into account the downstream change of Reynolds number in the study of the disturbance development, as has been essential in the studies of a Blasius boundary layer.

Finally, there is the fact that this flow supports more than one type of instability, depending upon the Reynolds number of the flow. The basis was presented by Lilly (1966). Although classical stability theory tends to focus on the problem of a critical Reynolds number, it should be recognized that a laminar flow may be established at a Reynolds number higher than the critical value. If the linear initial-value problem is to be used in understanding the initial stages of transition, it should be understood that these initial stages can differ for different values of Reynolds number.

2. Solution of the stability problem

The system under consideration is motion in a rotating, homogeneous, incompressible, viscous fluid. The appropriate equations of motion together with the incompressibility condition are

$$\left.\begin{aligned}
\frac{\partial \bar{u}}{\partial t}+\bar{u}\frac{\partial \bar{u}}{\partial x}+\bar{v}\frac{\partial \bar{u}}{\partial y}+\bar{w}\frac{\partial \bar{u}}{\partial z}-f\bar{v} &= \frac{-1}{\rho}\frac{\partial \bar{p}}{\partial x}+\nu\left[\frac{\partial^2\bar{u}}{\partial x^2}+\frac{\partial^2\bar{u}}{\partial y^2}+\frac{\partial^2\bar{u}}{\partial z^2}\right],\\
\frac{\partial \bar{v}}{\partial t}+\bar{u}\frac{\partial \bar{v}}{\partial x}+\bar{v}\frac{\partial \bar{v}}{\partial y}+\bar{w}\frac{\partial \bar{v}}{\partial z}+f\bar{u} &= \frac{-1}{\rho}\frac{\partial \bar{p}}{\partial y}+\nu\left[\frac{\partial^2\bar{v}}{\partial x^2}+\frac{\partial^2\bar{v}}{\partial y^2}+\frac{\partial^2\bar{v}}{\partial z^2}\right],\\
\frac{\partial \bar{w}}{\partial t}+\bar{u}\frac{\partial \bar{w}}{\partial x}+\bar{v}\frac{\partial \bar{w}}{\partial y}+\bar{w}\frac{\partial \bar{w}}{\partial z} &= \frac{-1}{\rho}\frac{\partial \bar{p}}{\partial z}+\nu\left[\frac{\partial^2\bar{w}}{\partial x^2}+\frac{\partial^2\bar{w}}{\partial y^2}+\frac{\partial^2\bar{w}}{\partial z^2}\right],\\
\frac{\partial \bar{u}}{\partial x}+\frac{\partial \bar{v}}{\partial y}+\frac{\partial \bar{w}}{\partial z} &= 0,
\end{aligned}\right\} \tag{2.1}$$

where $\bar{u}$, $\bar{v}$ and $\bar{w}$ are the velocities in the x-, y- and z-directions, respectively, and the co-ordinate system is right-handed with z directed positive upward. The other quantities are the pressure $\bar{p}$, the constant density ρ, the Coriolis parameter f and the kinematic viscosity ν. The unknown quantities are now regarded as being the sum of a mean and a fluctuating part, namely

$$\bar{u} = U+u, \quad \bar{w} = W+w, \quad \bar{v} = V+v, \quad \bar{p} = P+p. \tag{2.2}$$

The mean quantities are time-independent. The fluctuating portion is taken as a perturbation on that mean with the assumption that the amplitudes of the perturbations and the derivatives of these amplitudes are small enough to allow for linearization. Solutions of (2.1) for the time-independent mean flow form the familiar Ekman velocity profile or

$$\begin{aligned} U &= U_g[1-e^{-z(f/2\nu)^{\frac{1}{2}}}\cos(z(f/2\nu)^{\frac{1}{2}})], \\ V &= U_g e^{-z(f/2\nu)^{\frac{1}{2}}}\sin(z(f/2\nu)^{\frac{1}{2}}), \\ W &= 0, \end{aligned}$$

with U_g the geostrophic velocity.

The disturbance equations are formed by substituting the expressions in (2.2) into (2.1) and subtracting the mean flow. Ignoring all nonlinear terms, the following system results:

$$\left.\begin{aligned} \frac{\partial u}{\partial t}+U\frac{\partial u}{\partial x}+V\frac{\partial u}{\partial y}+w\frac{\partial U}{\partial z}-fv &= \frac{-1}{\rho}\frac{\partial p}{\partial x}+\nu\nabla^2 u, \\ \frac{\partial u}{\partial t}+U\frac{\partial v}{\partial x}+V\frac{\partial v}{\partial y}+w\frac{\partial V}{\partial z}+fu &= \frac{-1}{\rho}\frac{\partial p}{\partial y}+\nu\nabla^2 v, \\ \frac{\partial w}{\partial t}+U\frac{\partial w}{\partial x}+V\frac{\partial w}{\partial y} &= \frac{-1}{\rho}\frac{\partial p}{\partial z}+\nu\nabla^2 w, \\ \frac{\partial u}{\partial x}+\frac{\partial v}{\partial y}+\frac{\partial w}{\partial z} &= 0, \end{aligned}\right\} \tag{2.3}$$

with

$$\nabla^2 = \frac{\partial^2}{\partial x^2}+\frac{\partial^2}{\partial y^2}+\frac{\partial^2}{\partial z^2}.$$

The appropriate boundary conditions are

$$u = v = w = 0 \quad \text{at} \quad z = 0; \quad u, v, w \to 0 \quad \text{as} \quad z \to \infty.$$

The perturbations are now assumed to be of the form

$$u(x, y, z, t) = \hat{u}(z)\, e^{i(\alpha x+\gamma y-\omega t)}$$

(and similar forms for v, w, p). This solution form is a double Fourier decomposition (where α and γ are respectively the x- and y-components of the wavenumber vector) coupled with the normal-mode assumption (where ω is the complex frequency). Substituting into (2.3), non-dimensionalizing with the bases U_g, and the length scale $(\nu/f)^{\frac{1}{2}}$, and performing other operations yields a coupled set of ordinary differential equations, namely:

$$L(\hat{w}) = F(\tilde{u}), \quad M(\tilde{u}) = G(\hat{w}). \tag{2.4}$$

The operations required to obtain (2.4) are (*a*) change of variable and (*b*) elimination of the pressure. Specifically, in the (x, y)-plane ((α, γ)-plane) changing from Cartesian to polar co-ordinates allows

$$\tilde{\alpha}^2 = \alpha^2+\gamma^2, \quad \phi = \arctan(\gamma/\alpha), \tag{2.5}$$

with the definitions

$$\left.\begin{aligned} \tilde{\alpha}\tilde{u} &= \gamma\hat{u} - \alpha\hat{v}, \quad \tilde{\alpha}\tilde{U} = \gamma U - \alpha V, \\ \tilde{\alpha}\tilde{v} &= \alpha\hat{u} + \gamma\hat{v}, \quad \tilde{\alpha}\tilde{V} = \alpha U + \gamma V. \end{aligned}\right\} \tag{2.6}$$

The form (2.4) differs from that of Lilly (1966) on two counts. First, the angle ϕ used for orientation in the present work is the angle between the geostrophic velocity and the wavenumber vector. Lilly preferred the angle (ϵ in his notation) between the geostrophic velocity and the disturbance wave front. The two are related by $\phi = \epsilon + \frac{1}{2}\pi$.

Second, the length scale employed in the present work is $(\nu/f)^{\frac{1}{2}}$. Hence a factor of $\sqrt{\frac{1}{2}}$ different from the Lilly values must be expected. Accordingly, Reynolds numbers, wavenumbers and frequencies given herein must be multiplied by the factor $\sqrt{2}$ in order to make direct comparisons with the Lilly results.

The pair of equations (2.4) forms the basis for the analysis of this problem. These equations, along with the boundary conditions, form an eigenvalue problem that involves a relation between the Reynolds number R, the wavenumbers α and γ, and the complex frequency ω. Instability or stability depends upon whether or not the imaginary part of ω is positive or negative. In point of fact, the system (2.4) was combined to form one equation for $\hat{w}$, which was solved numerically using a standard shooting technique. On the other hand, the coupled pair facilitates both the discussion and the interpretation of the results. Comparison can, of course, be made with Lilly's presentation. The present method has, however, the advantage of allowing the application of the true boundary conditions at infinity for a disturbance in a boundary layer.

3. Discussion of the eigenvalues

Contours of real (ω_r) and imaginary (ω_i) parts of ω as a function of α and γ at fixed R are plotted in figure 1. These results are well documented by Lilly (1966), and the features of interest will be discussed briefly.

At $R = 45$, the contours of ω_i are roughly elliptical, centred around a single maximum at $\alpha = 0{\cdot}075$ and $\gamma = 0{\cdot}205$. This maximum is associated with a mode of instability that Lilly (1966) referred to as the parallel mode. It is technically a viscous mode in that it vanishes at high Reynolds numbers. (This statement should be interpreted as meaning that $\omega_i \to 0$ as $R \to \infty$.) The origin stems from rotation in the problem and energy is supplied by means of the component of mean shear that is parallel to the disturbance wave front.

At $R = 105$, the situation becomes more complicated. The region of instability is no longer a single ellipse, but instead the contours of ω_i show two maxima, one centred at $\alpha = 0{\cdot}037$, $\gamma = 0{\cdot}1948$ and a second centred at $\alpha = -0{\cdot}062$, $\gamma = 0{\cdot}3815$. The first extremum can still be shown to be associated with the parallel instability. The second appears to be associated with inflection points in the mean profile.

At $R = 350$, there is once again only a single maximum in the region of instability, centred at $\alpha = -0{\cdot}0818$ and $\gamma = 0{\cdot}34$. The mechanism of instability present at this Reynolds number is the inflection-point type and therefore inertial in origin.

4. Formal statement of the initial-value problem

Having examined the solutions to the classical stability problem, the growth and development of a more generalized disturbance will now be considered. Recall the perturbation equations for a small, fluctuating disturbance (2.3). The coefficients of this set of homogeneous differential equations are functions of z alone, and, if it is assumed that the perturbation quantities are absolutely integrable in the horizontal, (2.3) can be Fourier-transformed by

$$u(x, y, z, t) = \frac{1}{(2\pi)^2} \int_{-\infty}^{\infty} \int_{-\infty}^{\infty} \breve{u}(\alpha, \gamma; z, t)\, e^{i(\alpha x + \gamma y)}\, d\alpha\, d\gamma.$$

The inverse transformation is then

$$\breve{u}(\alpha, \gamma; z, t) = \int_{-\infty}^{\infty} \int_{-\infty}^{\infty} u(x, y; z, t)\, e^{i(\alpha x + \gamma y)}\, dx\, dy.$$

Similar expressions hold for v, w and p.

The transformed system still consists of partial differential equations in z and t. In order to solve the system, it is desirable to assume some form for the time dependence, resulting in a set of ordinary differential equations in z.

In the preceding discussion of the classical stability problem, it was noted that solutions of the problem could be obtained by the method of normal modes. That is, the perturbations were assumed to be solvable by a superposition of solutions of the form

$$\breve{u}(\alpha, \gamma; z, t) = \sum_{n=0}^{\infty} a_n\, \hat{u}_n(z; \alpha, \gamma)\, e^{-i\omega_n t}.$$

Such a substitution led to the eigenvalue problem, with ω playing the role of the eigenvalue. For a given set of α, γ and R, there may well be an infinite set of such eigenvalues. The a_n are amplitude coefficients determined by the initial conditions.

It should be noted that this form of solution does not necessarily yield the complete set of eigenvalues and eigenfunctions for the problem. If the time dependence is eliminated by means of a Laplace transform, the contour integral that must be inverted to find the time dependence of the solution may have contributions from sources other than the isolated singularities representing the normal modes. This aspect of the subject has not been exploited for this problem as has been done by Gustavsson (1979) for the Blasius layer, for example.

Presumably, if one possessed the entire set of eigenfunctions for this problem, was assured that they formed a complete set, and had the proper orthogonality conditions, a completely arbitrary initial disturbance could be represented as the properly weighted sum of those eigenfunctions, and its development could be traced. This most-general problem will not be addressed. Instead, several assumptions will be introduced because it is not possible to follow this route. In fact, an alternative problem must be posed.

First, although there may well be an infinite set of eigenvalues and, hence, eigenfunctions for a given set of parameters, only the most unstable mode will be considered. This means that all of the growing modes will be included. Such an approximation may lead to inaccuracies at early times, where any initial disturbance with a

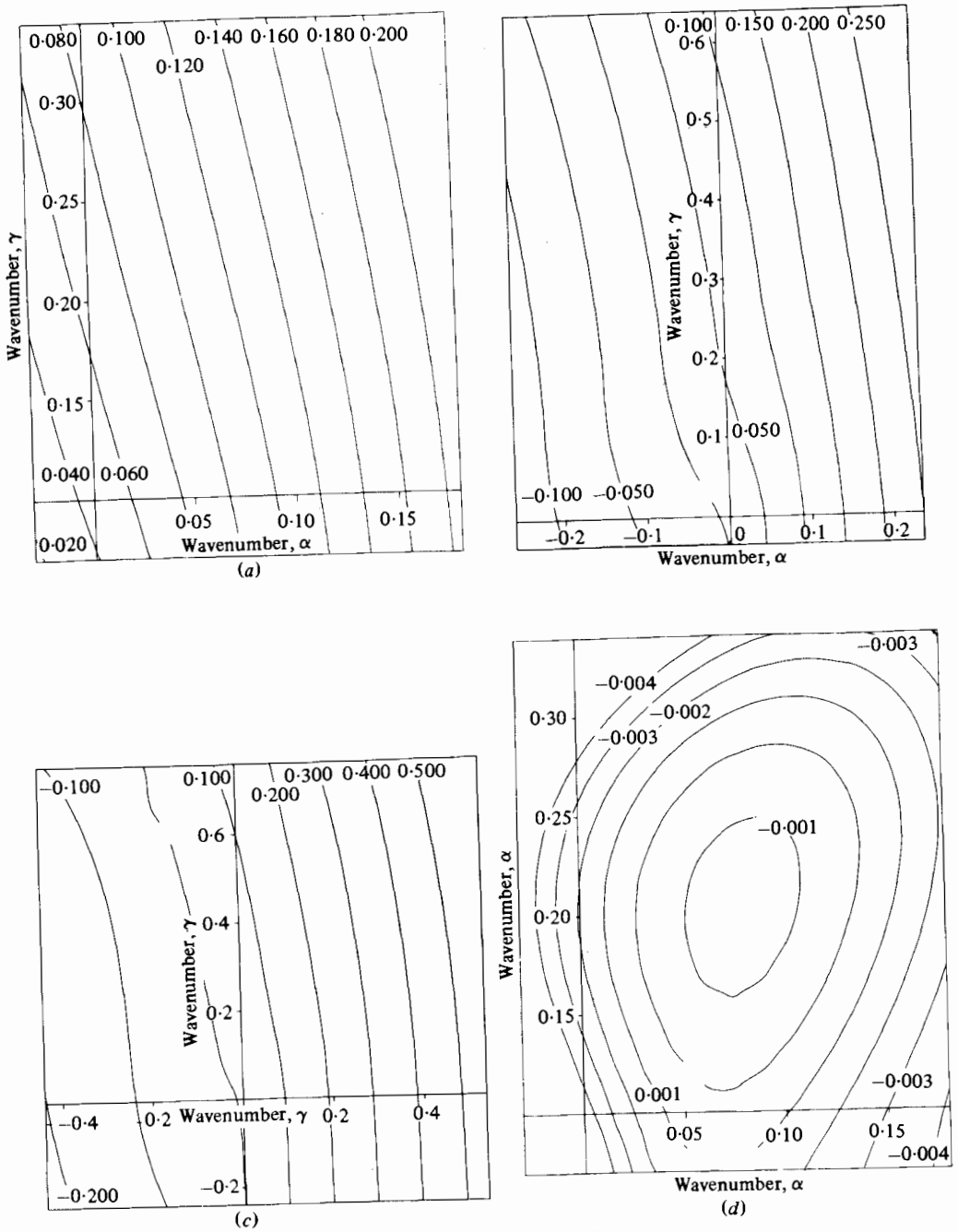

FIGURE 1. For legend see facing page.

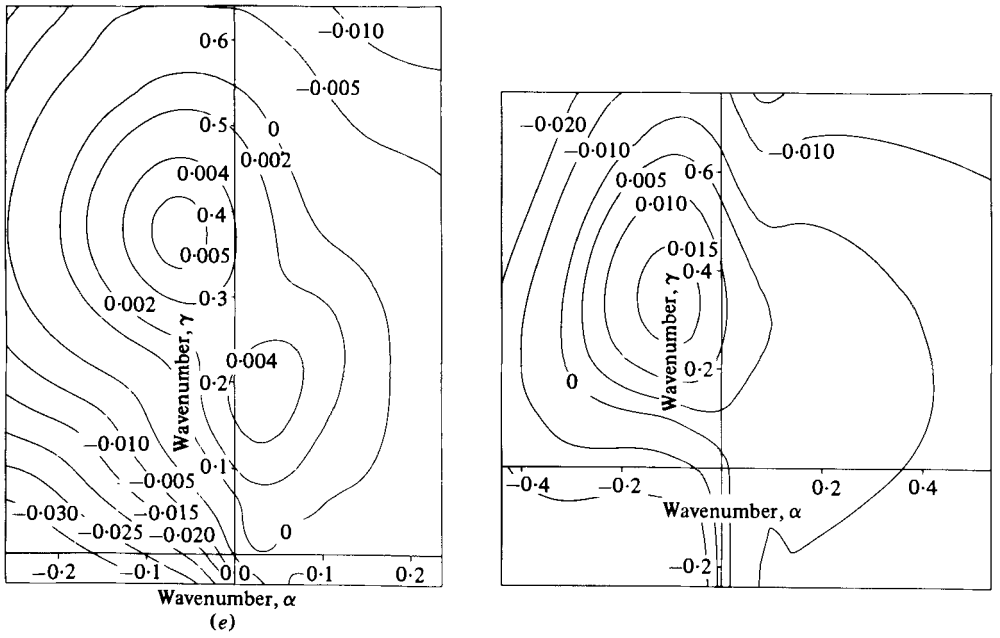

FIGURE 1. Contours of ω_r, for (*a*) $R = 45$, (*b*) 105, (*c*) 350; and of ω_i, for (*d*) $R = 45$, (*e*) 106, (*f*) 350.

given set of wavelengths may excite all possible modes of behaviour. Lack of knowledge about the eigenvalue spectrum along with its attendant eigenfunctions, however, makes this approximation necessary.

Second, the arbitrary z-dependence of the initial disturbance will have to be dropped. In effect, the disturbance will only be considered at a given level in the boundary layer. This is the same approach employed by Criminale & Kovasznay (1962) and Gaster (1975) in their studies of the initial-value problem in a Blasius boundary layer.

Finally, an input spectrum will be assumed such that the initial disturbance has the form of a pulse when describing the vertical velocity component. In its ideal form, the amplitude coefficients of the pulse will be non-biased across the Fourier spectrum. This suggested form will vary somewhat with the different approximations discussed, but, in all cases, the initial disturbance will very closely approximate a pulse at a given level in the flow. Of course, since the system is linear, any other generalized disturbance can be built up from the sum of the unit pulses.

5. Discussion of the short-time problem

It would be desirable to begin the analysis of the general problem by examining what occurs immediately after the inception of the initial disturbance. Unfortunately, it is at short times that the lack of knowledge about the entire set of eigenvalues is felt most severely. At such short times, before the damped modes have a chance to die out, the behaviour of all possible modes should be taken into account in order to give a true picture of the disturbance behaviour. The exact nature of all these modes is unknown for the Ekman problem. Mack (1976), Murdock & Stewartson (1977) and

R	α	$\Delta\alpha$	γ	$\Delta\gamma$
45	−0·030–0·180	0·03	−0·070–0·340	0·03
105	−0·260–0·235	0·045	−0·035–0·640	0·045
350	−0·440–0·535	0·065	−0·240–0·800	0·065

TABLE 1

R	$\Delta\alpha$	$\Delta\gamma$
45	0·015	0·015
105	0·014	0·014
350	0·020	0·020

TABLE 2

Gustavsson (1979) have examined the case of the Orr–Sommerfeld equation for the Blasius layer and have presented evidence that the eigenvalues consist of a continuous spectrum as well as the discrete set of eigenvalues. The present perturbation problem has many features in common with the Orr–Sommerfeld equation and therefore there is reason to suspect that a similar distribution of eigenvalues should exist for the Ekman layer. Clearly, the present state of knowledge concerning the distribution of eigenvalues for the Ekman problem is insufficient to present a detailed description of the disturbance at short times.

6. Intermediate time

For non-dimensional times between $t = 25$ and $t = 1000$, the initial disturbance was represented as a finite double Fourier series with amplitude coefficients identically equal to unity. Thus, in this aspect of the analysis, the input spectrum of the disturbance had a square-wave form, being of unit magnitude over the modes which were summed and assumed to be zero elsewhere. All growing modes were included. The form of the disturbance was therefore

$$w(x, y, t) = \sum_{\alpha}\sum_{\gamma} e^{i(\alpha x+\gamma y-\omega t)}. \tag{6.1}$$

This expression for w was evaluated directly over the range of wavenumbers at the spacings given in table 1.

A signal represented by a series of the form $\Sigma_{n=0}^{N} \cos(A_0 + n\Delta A)x$ will be aliased over a distance $2\pi/\Delta A$. Since the set of eigenvalues given above was to be used to calculate w in the (x, y)-plane, it was desirable to have this distance large enough to prevent distortion of the plots by aliasing. To accomplish this, the set of eigenvalues was interpolated by means of a standard interpolation routine available in the software package of the National Maritime Institute, England. A new set of eigenvalues was produced with identical ranges but smaller spacings; see table 2.

Such a procedure is not entirely free from undesirable consequences. The interpolation is being performed under the assumption that the known eigenvalues give a good representation of the eigenvalue surface as a function of R, α and γ, and that

this surface is sufficiently smooth to allow accurate portrayal by the set of interpolated eigenvalues. Since it is not expected that such an interpolation will yield eigenvalues to the accuracy of those calculated directly by integration, the procedure will, in fact, introduce inaccuracies. Interpolation was the only practical method for extending the eigenvalue set, however, as direct calculation of the eigenvalues was quite time-consuming. It is felt that distortions caused by the use of this process will be minimal.

A further possibility of inaccuracy lies in representing by means of a finite Fourier series a phenomenon which is actually a Fourier integral. The truncation of the series, for example, results in a 'ringing' present at short times. As a result, the presence of small-amplitude waves appearing to propagate out from the wave packet are clearly visible. These distortions disappear as time increases and the growth of the amplitude coefficients causes a smoothing of the ends of the Fourier spectrum.

There is also the fact that such a disturbance is really not the sum of discrete modes, and, as such, would differ from the Fourier-series representation of its measured signal.

Interpolation was also necessary to create the perspective plots of w obtained by evaluating (6.1) over the given ranges of α and γ. The original grid of points in the (w, y)-plane proved too sparse to obtain fine detail in the representation of the wave packet. Closely spaced lines in the perspective plot are necessary to obtain this detail by means of a shadowing effect. The values of (6.1) were therefore interpolated by means of the same program used to interpolate the eigenvalues. The spacing of grid points in the (x, y)-plane was halved, thus producing a much more satisfactory representation of the wave packet.

Figure 2 shows the results for three different times in each of the three Reynolds-number cases. These are perspective plots of $w(x, y, t)$ at a given level of the flow. The dependence of the initial-value problem on Reynolds number is clearly revealed.

For $R = 45$, much of the pulse-like nature of the disturbance has already been lost by $t = 25$. This is due, in part, to the relatively few modes included in the summation (actual count is 285). On the other hand, the region of instability for this Reynolds number is much smaller than those for higher values, and, since only a relatively few modes do not dampen, what is seen is representative of the nature of the region of instability.

For short time, the dominant wave will be the one whose wavenumbers are located at the centre of the rectangular input spectrum. The location coincides closely with the most growing mode for the $R = 45$ case. As time progresses, therefore, little change is observed in the lines of constant phase. The orientation remains almost constant and represents the most growing mode; in the $R = 45$ case, it is the parallel mode. The contours of the modulus of the wave packet develop toward oblique ellipses.

At $R = 105$, both the inflection point and the parallel modes are present and the double maxima are mirrored in the development of the disturbance. As time progresses, the disturbance takes on the form of two overlapping wave packets, one representing the inflection-point mode and the other representing the parallel mode.

By $R = 350$, only the inflection-point mode is present. The large area of instability results in a disturbance with a bowed appearance at times less than about $t = 300$ but, after that, the disturbance again assumes the form of an elliptical wave packet whose dominant wave is the most growing.

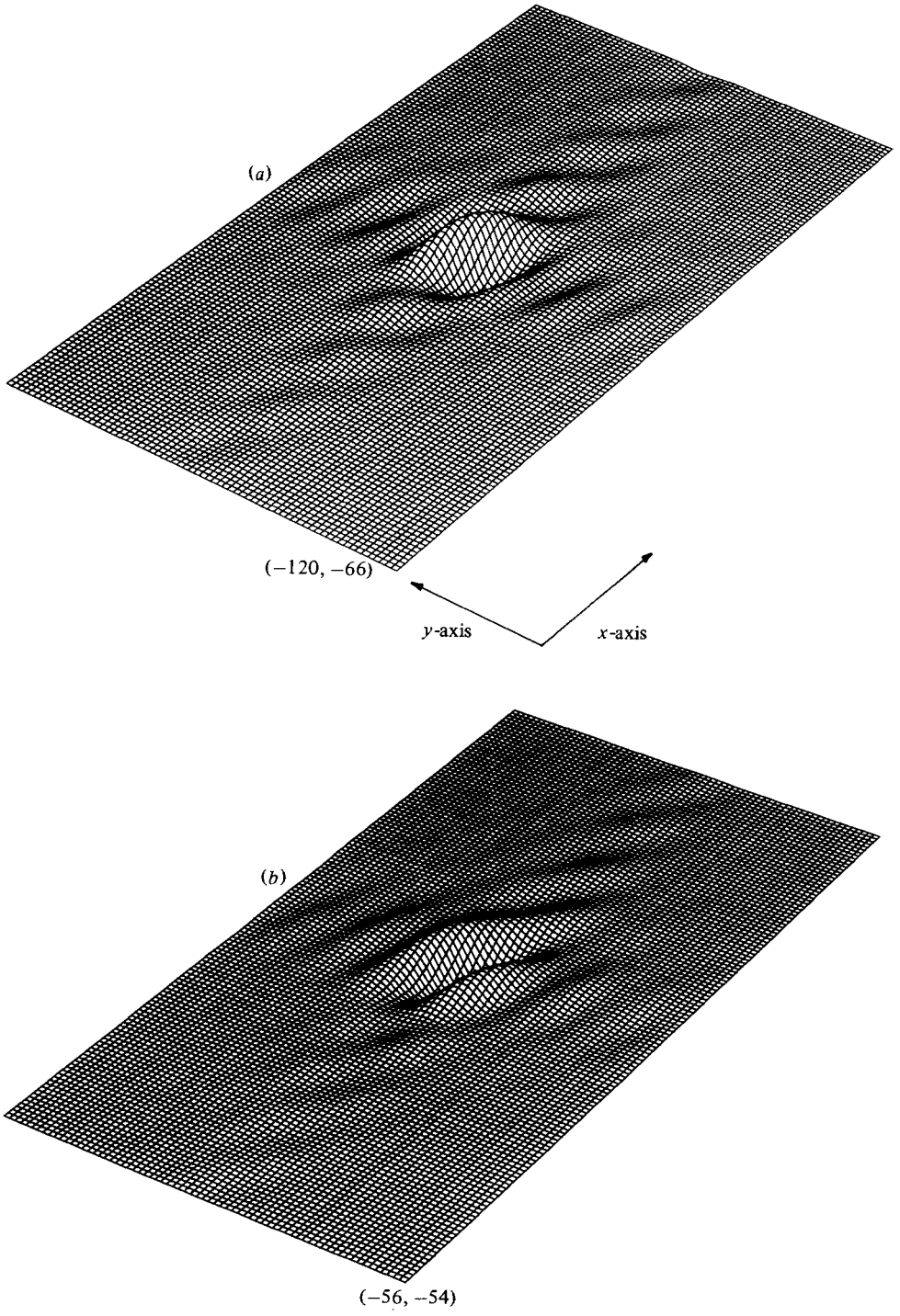

FIGURE 2. For legend see p. 340.

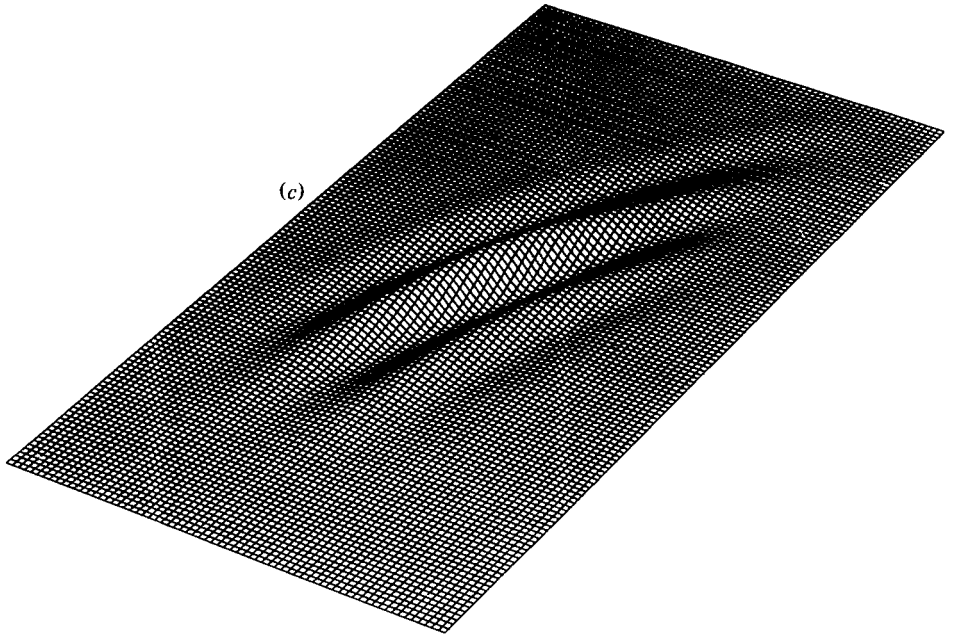

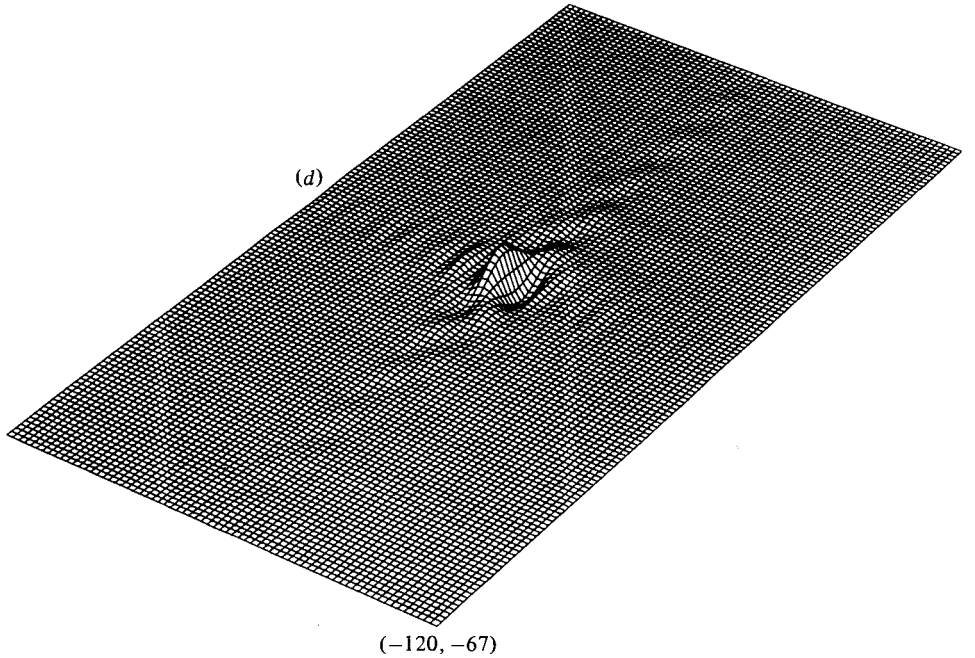

FIGURE 2. For legend see p. 340.

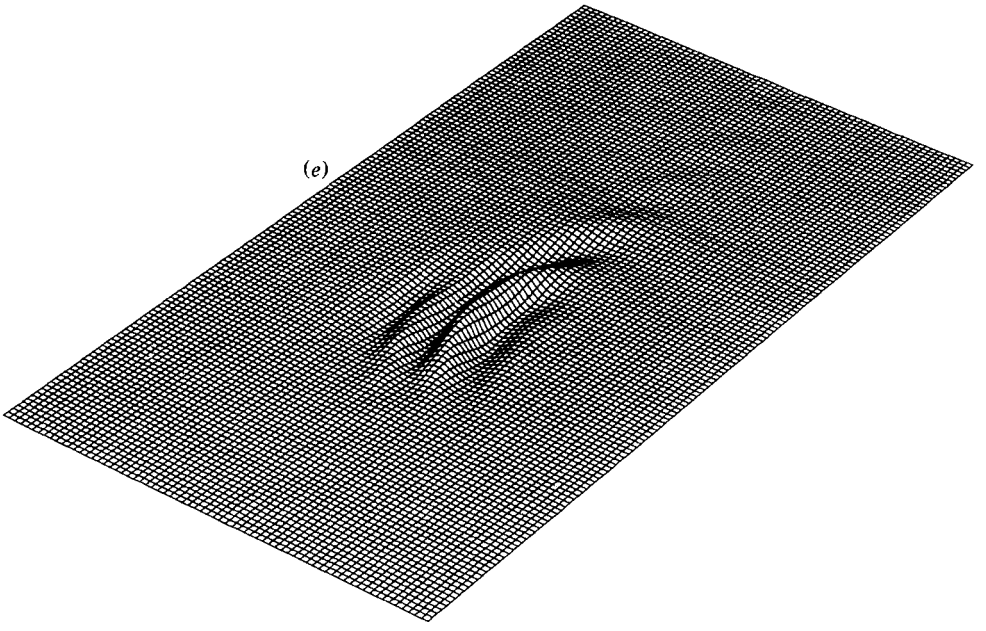

(34, −43)

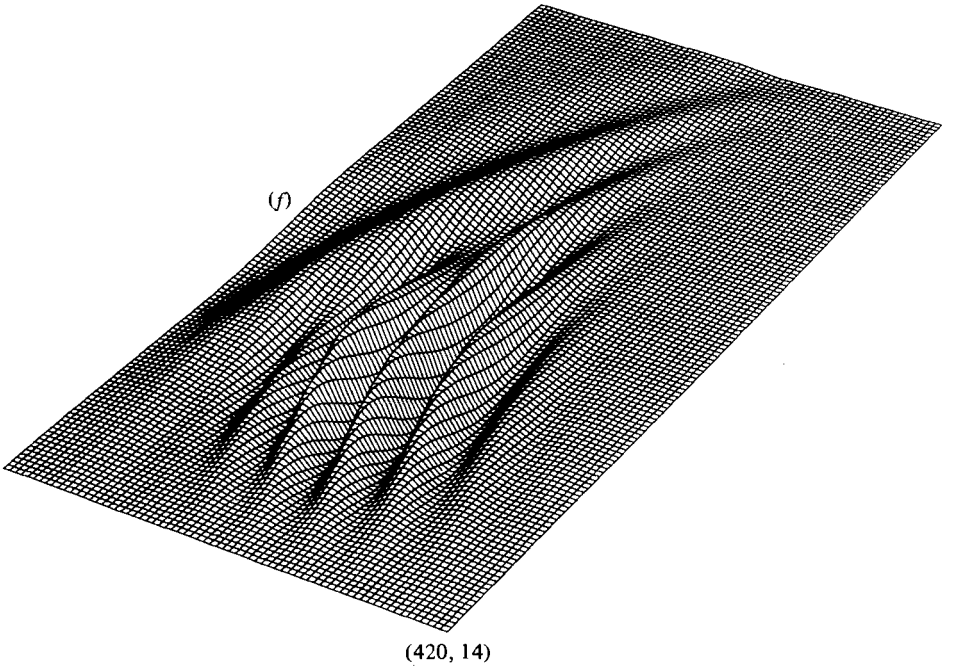

(420, 14)

FIGURE 2. For legend see p. 340.

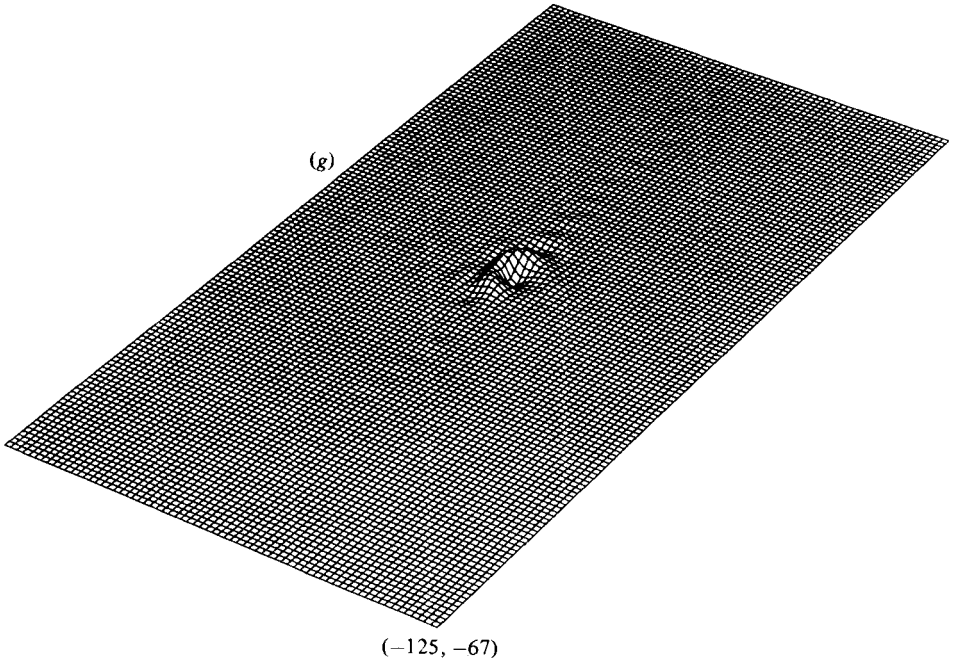

FIGURE 2. For legend see p. 340.

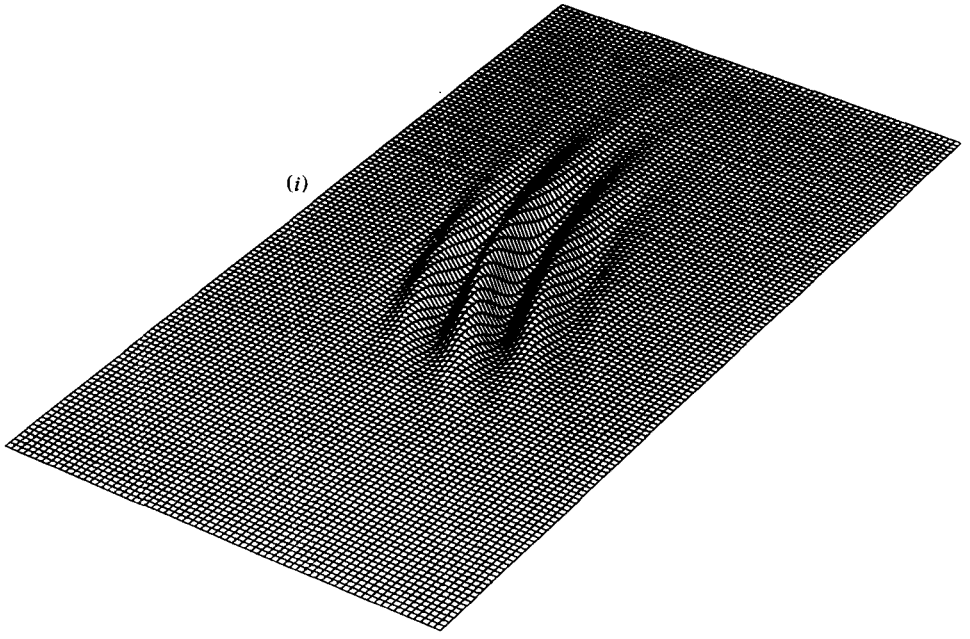

FIGURE 2. Perspective plots of w, for different values of R and of the non-dimensional time t. (*a*) $R = 45$, $t = 25$; (*b*) 45, 400; (*c*) 45, 700; (*d*) 105, 25; (*e*) 105, 200; (*f*) 105, 700; (*g*) 350, 25; (*h*) 350, 300; (*i*) 350, 400. The horizontal co-ordinates of the lower right-hand corner of the grid are given in units of non-dimensional length with respect to the centre of the disturbance at $t = 0$. A grid space represents two units of non-dimensional length.

7. Asymptotic evaluation

It is now desired to evaluate the integral

$$\int_{-\infty}^{\infty}\int_{-\infty}^{\infty} a(\alpha,\gamma)\, e^{i(\alpha x+\gamma y-\omega(\alpha,\gamma)t)}\, d\alpha\, d\gamma,$$

for very large time. For purposes of the analysis, it will be possible for the disturbance to have the form of a true pulse. The amplitude coefficients will be totally non-biased initially, and a flat input spectrum will be assumed. The initial amplitude $a(\alpha,\gamma)$ will therefore be identically equal to unity.

It is reasonable to assume that analytic continuation will allow ω to be written as a complex function of the now complex parameters α and γ. The integral may then be taken over a contour in complex (α,γ)-space and written as

$$I = \int_{-\infty}^{\infty}\int_{-\infty}^{\infty} \exp\left[i\left(\alpha\frac{x}{t}+\gamma\frac{y}{t}-\omega_r-i\omega_i\right)t\right] d\alpha\, d\gamma.$$

The integral is now in a suitable form to apply the method of steepest descent (see e.g. Erdélyi 1956). This results in the following approximation for I:

$$I \simeq C_1 \frac{\pi}{t(A_1B_1)^{\frac{1}{2}}},$$

where
$$-A_1 = \left[\tfrac{1}{2}\cos^2\theta\frac{\partial^2\omega_i}{\partial\alpha_r^2} + \tfrac{1}{2}\sin^2\theta\frac{\partial^2\omega_i}{\partial\gamma_r^2} + \cos\theta\sin\theta\frac{\partial^2\omega_i}{\partial\alpha_r\partial\gamma_r}\right],$$

$$-B_1 = \left[\tfrac{1}{2}\sin^2\theta\frac{\partial^2\omega_i}{\partial\gamma_r^2} + \tfrac{1}{2}\cos^2\theta\frac{\partial^2\omega_i}{\partial\gamma_r^2} - \cos\theta\sin\theta\frac{\partial^2\omega_i}{\partial\alpha_r\partial\gamma_r}\right],$$

$$C_1 = \exp it\left[\alpha_0\frac{\partial\omega_r}{\partial\alpha_r} + \gamma_0\frac{\partial\omega_r}{\partial\gamma_r} - \omega_0\right],$$

$\omega_0 = \omega(\alpha_0, \gamma_0)$ or the saddle-point location.

Here $\theta = \arctan m$, where m is the tangent of an acute angle and is a solution of the following quadratic equation:

$$\frac{1}{2}\left[\frac{\partial^2\omega_i}{\partial\alpha_r\partial\gamma_r}\right]m^2 + \left[\frac{\partial^2\omega_i}{\partial\alpha_r^2} - \frac{\partial^2\omega_i}{\partial\gamma_r^2}\right]m - \frac{1}{2}\left[\frac{\partial^2\omega_i}{\partial\alpha_r\partial\gamma_r}\right] = 0.$$

The derivatives are evaluated at (α_0, γ_0).

Lack of information on the complete complex dispersion relation restricts this method to real values of x/t and y/t. Thus the only information which can be obtained lies along rays representing modes whose growth rates are extrema in real wavenumber space. Along such rays, where

$$\frac{x}{t} = \frac{\partial\omega_r}{\partial\alpha_r}\bigg|_{(\alpha_0,\gamma_0)}, \quad \frac{y}{t} = \frac{\partial\omega_r}{\partial\gamma_r}\bigg|_{(\alpha_0,\gamma_0)},$$

the wave has an amplitude inversely proportional to time. It will have wavenumbers and frequency equal to α_0, γ_0 and ω_0, respectively.

More information can be obtained with a slight relaxation of rigour. If α and γ are once again considered to be real parameters, a simple expansion about the maximum value of ω_i yields the following expression:

$$I \simeq \frac{e^{i[\alpha_0 x + \gamma_0 y - \omega_0 t]}}{t(A_1 B_1)^{\frac{1}{2}}} e^{-\bar{x}/4A_1 t} e^{-\bar{y}/4B_1 t}.$$

A_1, B_1 and θ are as previously defined, while

$$\bar{x} = \left(x - \frac{\partial\omega_r}{\partial\alpha}t\right)\cos\theta + \left(y - \frac{\partial\omega_r}{\partial\gamma}t\right)\sin\theta,$$

$$\bar{y} = -\left(x - \frac{\partial\omega_r}{\partial\alpha}t\right)\sin\theta + \left(y - \frac{\partial\omega_r}{\partial\gamma}t\right)\cos\theta.$$

The above expression shows that the asymptotic wave packet is an ellipse whose axes are parallel to the rotated co-ordinate axes $\bar{x}$ and $\bar{y}$. The ratio of the axis in the $\bar{x}$-direction to that in the $\bar{y}$-direction is

$$\epsilon = (A_1/B_1)^{\frac{1}{2}}.$$

8. Summary of results of the initial-value problem

The preceding sections have made use of several different approximations in order to determine the time behaviour of a pulse-like initial disturbance. Any other small-amplitude initial disturbance can be formed by superposition of such pulses.

With this accomplished, it is now possible to answer the following general questions for the problem.

(1) What is the initial change in the form of the disturbance?

(2) What is the time development of the significant bandwidth of the disturbance in wave space?

(3) How quickly does the initial disturbance assume the form dictated by the most growing mode?

(4) What is the group velocity of the disturbance?

(5) What is the asymptotic form that the disturbance can be expected to assume?

(6) How do the above questions depend upon the Reynolds number?

Although lack of information precludes a detailed analysis of the short-time behaviour of an initial disturbance, an educated guess as to the general form of this behaviour can be made. If a very flat initial spectrum is assumed, there will be a large amount of energy present in damped modes. This energy will decrease after $t = 0$, and the growing modes will be unable to compensate for the loss immediately. The loss of energy will have two effects. First, it will cause an initial drop in the amplitude of the disturbance. Secondly, it will effectively decrease the bandwidth of the amplitude spectrum, resulting in a spreading of the pulse in physical space.

In the case of a Blasius laminar boundary layer, the most-amplified disturbance does not have a cross-stream component in its wavenumber vector. Thus, a pulse imposed upon such a mean flow will ultimately assume the form of a wave packet whose component waves have crests perpendicular to the mean flow and possess the physical characteristics of the most-growing wave, nonlinearities permitting. An important question in this case is: how quickly does the initial disturbance assume this form? While such two-dimensionality is precluded in the present case, both by the nature of the mean flow and by the orientation of the most-amplified waves, it is nevertheless of interest to examine the questions of how quickly the disturbance approaches the forms dictated by the most-growing modes.

In the case of an idealized pulse with a non-biased initial amplitude of unit value, the amplitude spectrum of the disturbance will have the form

$$A(\alpha, \gamma) = e^{\omega_i(\alpha,\gamma)t}.$$

Thus, for any time greater than $t = 0$, the maximum values of A will be located at the point or points in wavenumber space that represent maxima of ω_i. These maxima, therefore, cannot be used to indicate how quickly the disturbance is approaching the state dictated by them. A better indicator of this behaviour is the bandwidth of the amplitude spectrum around the most-amplified modes. As time progresses, differential growth will cause the amplitude of this area to assume greater and greater relief. Contributions to the disturbance, then, can be regarded as coming from a localized region surrounding these modes. The smaller the region becomes, the more the disturbance will resemble a wave train of the most-growing waves. The inverse of the bandwidth can also be thought of as an indication of how many oscillations are contained in the wave packet.

The $A^2(\alpha, \gamma) = 0{\cdot}3$ contours of the power spectra normalized on the maximum value were chosen to represent the bandwidth of the disturbance. This is slightly lower in value than a contour representing the e-folding distance of the distribution

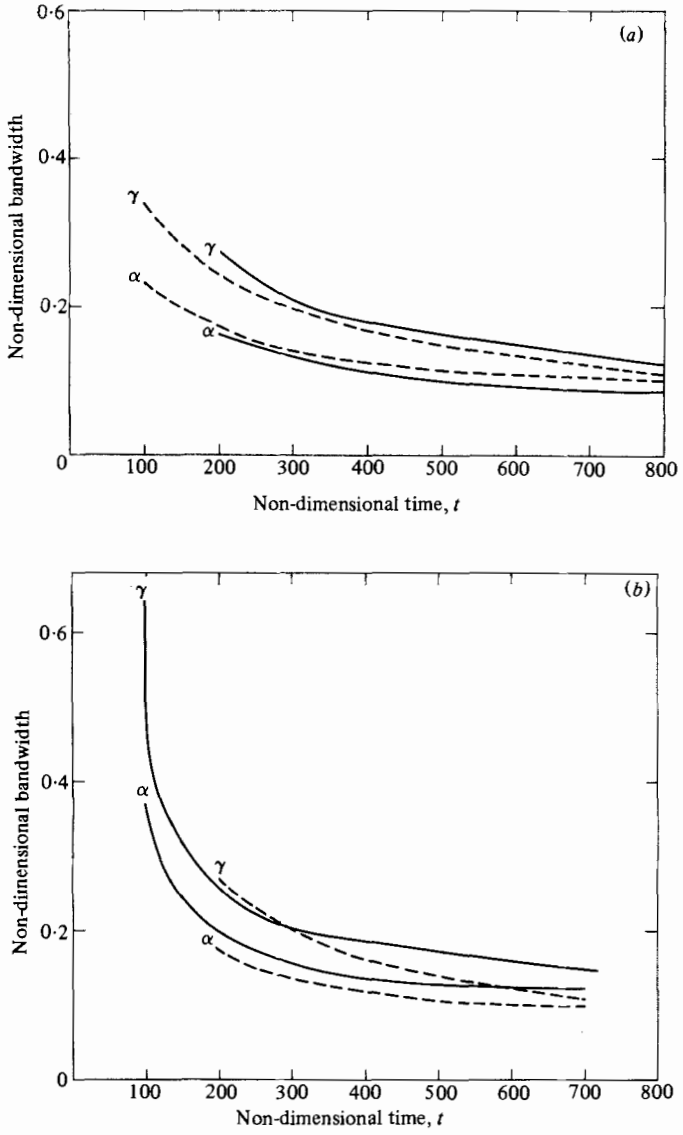

FIGURE 3. Wave-packet bandwidths for (*a*) $R = 45$ (——) and 350 (– – –); (*b*) $R = 105$ (——, mixed mode; – – –, parallel mode).

($e^{-1}A_{\max} = 0{\cdot}37A_{\max}$). Figure 3 shows plots of the bandwidths of these contours in the α- and γ-directions.

Two items of interest can be obtained from these plots. First, it can be seen that in all cases, while there is an initial period in which the drop in the bandwidth is rather rapid, the rate of decrease slows considerably for larger times. A notable bandwidth remains at $t = 700$, indicating that at none of the Reynolds numbers is there a close approach to a pure wave train. This conclusion is, of course, substantiated by examination of the perspective plots. The width does approach zero at $t \to \infty$, however, as is to be expected.

The second item is that, at all three Reynolds numbers, the bandwidth in γ remains

R	V_{gx}	V_{gy}	V_{px}	V_{py}
45 (parallel mode)	0·798	0·229	0·195	0·536
105 (parallel mode)	0·683	0·166	0·078	0·402
105 (inflection-point mode)	0·721	0·114	−0·010	0·065
350 (inflection-point mode)	0·610	0·108	0·019	−0·004

TABLE 3. Components of the group velocities V_g of the wave packets and the phase velocities V_p of the most-amplified modes. The x-axis is aligned with the geostrophic flow.

larger than that in α. This indicates that the wave packet thus represented will be elongated in the direction of the free stream. This is in contrast to the wave packets formed from a pulse in the Blasius layer. These packets are elongated in the cross-stream direction.

While the behaviour of the bandwidth in wave space serves to indicate that the approach to a wave train is slow, examination of the perspective plots indicates that the adoption of the orientation and spacing of the most-growing mode by the individual waves in the packet is rather more rapid. The ultimate alignment occurs most quickly for low Reynolds number, where it has taken place by $t = 300$. While the overall picture occurs in the manner described, it is the group velocity which more generally governs the motion of the wave packets. Asymptotically, the packets move with this velocity, $\mathbf{V}_g$, with components $(\partial\omega_r/\partial\alpha, \partial\omega_r/\partial\gamma)$ defined at the point in (α, γ)-space where ω_i is a maximum. The packets travel with velocities closely approaching these values even before the asymptotic state has been reached. Table 3 gives the components of the group velocities of the respective packets at different Reynolds numbers, along with the phase-velocity components of the most-growing modes.

Regardless of the Reynolds number, the group velocity is almost parallel to the free-stream velocity. Noteworthy is what occurs at $R = 105$. It was originally thought that the presence of two separate modes of instability at this Reynolds number would give rise to a pair of wave packets that would disperse and go their separate ways. Instead, the fact that the group velocities of the two different modes are essentially equal, coupled with the fact that both wave packets spread in time, results in a rather different picture. Instead of the two separate packet portions, calculations up to $t = 1000$ reveal a single patch of disturbance, consisting of two overlapping packets. Consequently, indications are that there will not be a total separation.

A further comment concerns the drop in $|\mathbf{V}_g|$ with Reynolds number. Such a variation is a result of the change in distribution of growth rates with Reynolds number.

Finally, information can be obtained from the asymptotic analysis. The ratio between the minor axis and the major axis of the asymptotic ellipse can be calculated through the use of the quantity ϵ in §7. This ratio ϵ^* is given in table 4.

The asymptotic forms of the disturbance can be employed to obtain an idea of the spreading rate of the packet. As a measure of the rate, the amount of time needed for the packet to spread a distance of 10 wavelengths of the most-amplified mode can be calculated. Two spreading times result, one for the spreading perpendicular to the wave crest, T_1, and one for the spreading parallel to the wave crest, T_2. If the border of the packet is designated as the line where the modulus falls to $e^{-\pi}$ of the maximum value, the results shown in table 5 are obtained.

R	ϵ^*
45 (parallel mode)	0·623
105 (parallel mode)	0·675
105 (inflection-point mode)	0·738
350 (inflection-point mode)	0·667

TABLE 4. Ratio of the minor axis to the major axis of the asymptotic ellipse

R	T_1	T_2
45 (parallel mode)	8246	3197
105 (parallel mode)	7432	3383
105 (inflection-point mode)	2859	1556
350 (inflection-point mode)	3484	1548

TABLE 5. Time to spread ten wavelengths of the most-amplified mode in the direction perpendicular to the wave front, T_1, and parallel to the wavefront, T_2

R	T_1
45 (parallel mode)	8825
105 (parallel mode)	6656
105 (inflection-point mode)	9731
350 (inflection-point mode)	9731

TABLE 6. Absolute spreading rates perpendicular to the wave front

The parallel modes take noticeably longer to spread 10 of their wavelengths. In a way, this is deceiving because these wavelengths are much larger for the parallel modes than they are for their inflection-point counterparts. If a designated half-width, 150 say, is used to compare spreading rates, a better idea of the relative rates of spreading can be obtained. This is done in table 6 for T_1.

The disturbances resulting from the parallel modes are actually spreading more quickly than those due to the other modes. There seems to be little difference in the spreading rates of the inflection-point mode at $R = 105$ and that at $R = 350$.

Finally, it was noted that the actual amplitude of the asymptotic wave packet is proportional to the inverse time. This is a standard asymptotic result for a double integral with the functional behaviour displayed herein.

The work was supported by the Air Force Office of Scientific Research under grant number F49620-79-C-0184 and the National Science Foundation under grant number OCE78-17677. The authors are also grateful to Dr M. Gaster for his valuable assistance with certain aspects of this work and the National Maritime Institute for its hospitality and support.

REFERENCES

BENJAMIN, T. B. 1961 *J. Fluid Mech.* **10**, 401.
CRIMINALE, W. O. 1960 *AGARD Rep.* no. 226.
CRIMINALE, W. O. & KOVASZNAY, L. S. G. 1962 *J. Fluid Mech.* **14**, 59.
ERDÉLYI, A. 1956 *Asymptotic Expansions.* Dover.
GASTER, M. & DAVEY, A. 1968 *J. Fluid Mech.* **32**, 801.
GASTER, M. & GRANT, I. 1975 *Proc. R. Soc. Lond.* A **347**, 253.
GUSTAVSSON, L. H. 1979 *Phys. Fluids* **22**, 1602.
KLEBANOFF, P. S., TIDSTROM, K. D. & SARGENT, L. M. 1962 *J. Fluid Mech.* **12**, 1.
LILLY, D. K. 1966 *J. Atmos. Sci.* **23**, 481.
MACK, L. 1976 *J. Fluid Mech.* **73**, 497.
MURDOCK, J. W. & STEWARTSON, K. 1977 *Phys. Fluids* **20**, 1404.
SCHLICHTING, H. 1935 *Nachr. Ges. Wiss. Göttingen* (*Neue Folge*) **1**, 4.
SCHUBAUER, G. B. & SKRAMSTAD, H. K. 1948 *N.A.C.A. Rep.* no. 909.